Polymer Degradation and Stability 246 (2026) 111924

Contents lists available at ScienceDirect

Polymer Degradation and Stability

journal homepage: www.journals.elsevier.com/polymer-degradation-and-stability

A nitrogen-oxygen triazine flame retardant for simultaneously improving flame retardancy and mechanical performance of nylon 6

Ruiqi Liu [a], Bin Tao [a], Suliang Gao [a], Miaojun Xu [a,*], Siqi Huo [b,*], Xiaoli Li [a], Bin Li [a,*]

[a] Heilongjiang Key Laboratory of Molecular Design and Preparation of Flame Retarded Materials, College of Chemistry, Chemical Engineering and Resource Utilization, Northeast Forestry University, Harbin, 150040, China
[b] School of Engineering, Centre for Future Materials, University of Southern Queensland, Springfield 4300, Australia

ARTICLE INFO

Keywords:
Polyamide 6
Nitrogen-oxygen flame retardant
Flame retardancy
Mechanical properties
Flame-retardant mechanism

ABSTRACT

The rapid advancement of modern industries has placed higher demands on the comprehensive performance of nylon 6 (PA6) and addressing its flammability issue has also received significant attention. Therefore, developing flame-retardant PA6 with superior overall performance has become a key research objective. In this work, a novel and highly efficient triazine-based flame retardant, phthalimidoxy-1,3,5-triazine (TPT), was successfully synthesized, and it was found to have a radical quenching mechanism analogous to that of hindered amine light stabilizers (HALS). Incorporating only 1.5 wt% TPT significantly improved the limiting oxygen index (LOI) of PA6/1.5TPT to 28% and increased both tensile strength and flexural strength to 80.49 and 93.25 MPa, respectively. Compared to pure PA6, the time to ignition (TTI) of PA6/1.5TPT was extended by 46.7%, and the total smoke production (TSP) was reduced by 42%. The hygrothermal aging results demonstrated that the PA6 composites maintained outstanding flame-retardant performance and mechanical integrity even after aging. Moreover, density functional theory (DFT) calculations and gas-phase mechanism analysis indicated that TPT generated stable radicals during thermal decomposition, which effectively captured hydrogen (H·) and carbon (C·) radicals produced in the initial degradation stage of PA6, thereby suppressing the combustion. This work presents a promising strategy for creating high-efficiency, multifunctional flame retardants for PA6, thus broadening its application potential.

1. Introduction

Nylon 6 (PA6), as an engineering polymer material with exceptional comprehensive properties, is extensively utilized in various fields including automotive components, electronic devices, medical equipment, and textiles [1–5]. However, its inherent flammability significantly restricts its application, and thus flame-retardant modification of PA6 crucial for enabling its broader and safer use [6,7]. Although halogen-based flame retardants exhibit high efficiency, they release substantial amounts of toxic gases during combustion, posing severe risks to human health and the environment [8,9]. Consequently, halogen-free flame retardants have emerged as a primary solution in academia and industry. The main mechanisms of halogen-free flame retardancy include radical scavenging [10], char formation and intumescence [11,12], and endothermic decomposition [13].

Polymer combustion is fundamentally a highly vigorous free radical chain reaction process [14], and thus free radical scavenging is one of the most intrinsic and efficient strategies to achieve flame retardancy. In recent years, HALS have attracted increasing research interest due to their distinctive free radical trapping mechanism [15–17]. HALS constitute a class of sterically hindered organic amine compounds, predominantly derived from 2,2,6,6-tetramethylpiperidine [18–20], and they are widely employed in polyolefin-based thin films owing to their outstanding anti-aging performance [21,22]. Studies have demonstrated that the primary mode of action involves the oxidation of hindered amines by reactive oxygen species to produce nitroxyl radicals. These radicals effectively scavenge propagating free radicals responsible for polymer degradation, forming transient quaternary ammonium salts. Subsequent decomposition of these intermediates yields stable alcohols and ketones while regenerating the nitroxyl radicals, thereby enabling a catalytic cycle that continuously suppresses the free radical chain propagation. Owing to this self-sustaining mechanism, HALS have emerged as highly promising candidates for flame-retardant applications in polymeric materials.

* Corresponding authors.
E-mail addresses: xumiaojun@nefu.edu.cn (M. Xu), Siqi.Huo@unisq.edu.au (S. Huo), libin82192699@nefu.edu.cn (B. Li).

https://doi.org/10.1016/j.polymdegradstab.2026.111924
Received 30 November 2025; Received in revised form 2 January 2026; Accepted 4 January 2026
Available online 5 January 2026

Wang et al. [23] synthesized a triazine-based flame retardant (NOR) and incorporated it into polypropylene. With only 2 wt % of NOR, the polypropylene composite achieved a (Vertical Thin Material Burning Test) VTM-0 rating, with an LOI of 27.3 %. Besides well-maintained mechanical properties, both peak heat release rate (PHRR) and total heat release (THR) were significantly decreased by 66.7 %. In addition, HALS can also function as synergists to enhance flame-retardant performance. Xie et al. [24] combined Flamestable NOR116 with an intumescent flame retardant (IFR) in polypropylene. When the loading level of IFR was 25 wt %, polypropylene only reached a vertical burning (UL-94) V-1 rating with an LOI of 31 %. However, substituting 0.5 wt % of IFR with Flamestable NOR116 enabled the material to achieve a UL-94 V-0 rating and an LOI of 35 %, demonstrating a significant synergistic effect between NOR116 and IFR.

At present, HALS have been applied primarily in polyolefin systems, and their effectiveness and mechanisims in PA6 have received only limited investigation. Notably, PA6 generates reactive species such as alkyl and alkoxy radicals during thermo-oxidative degradation [25–27], suggesting that HALS may theoretically exert flame retardant effects through radical quenching. Bianca Spieß et al. [28] synthesized a series of oxyimide compounds and incorporated them into PA6. Although the flame retardancy was enhanced, these oxyimide compounds generally exhibited inadequate thermal stability, rendering them incompatible with the high processing temperatures of PA6, limiting their practical values.

This work innovatively integrated nitrogen-oxygen structures with triazine ring, synthesizing a novel triazine-based nitrogen oxide compound (TPT) with exceptional thermal stability. The flame-retardant and mechanical properties of the resultant PA6/TPT composites were systematically evaluated, and the flame-retardant and enhancement mechanisms were comprehensively elucidated, thereby providing both theoretical insights and practical guidance for the design of highly effective, multifunctional nitrogen-oxygen-based flame retardants for PA6.

2. Experiment

2.1. Materials

Nylon 6 (PA6), grade 7331 J NC010, was procured from DuPont, USA. N—Hydroxyphthalimide (NHPI) and cyanuric chloride (TCT) were both purchased from Shanghai Yien Chemical Technology Co., Ltd

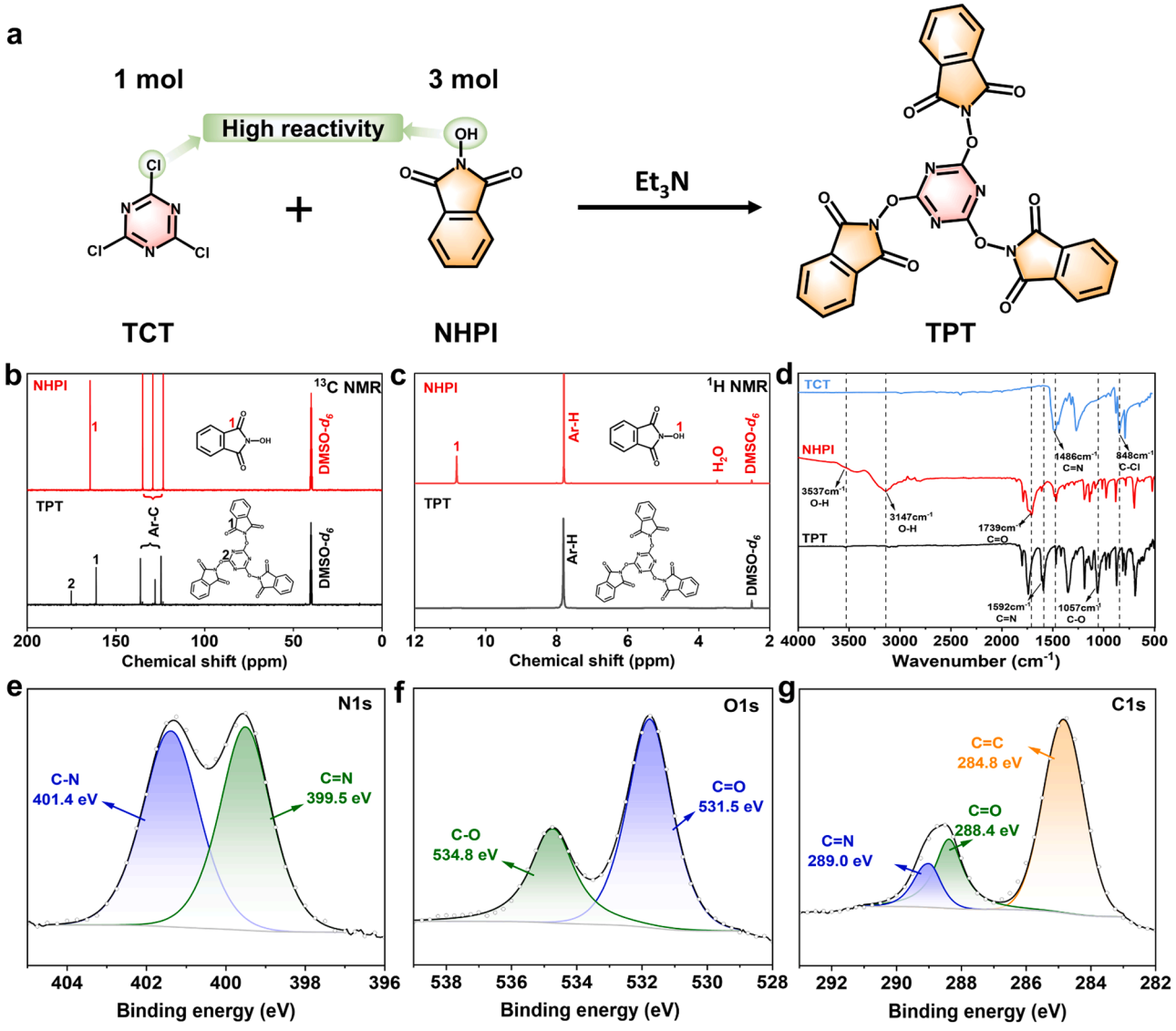

Fig. 1. (a) Synthesis of TPT; (b) ^{13}C and (c) ^{1}H NMR spectra of TPT; (d) FTIR spectra of TCT, NHPI and TPT; and XPS high-resolution (e) N1s, (f) C1s and (g) O1s spectra of TPT.

(China). Triethylamine (TEA) was provided by Tianjin Tianli Chemical Reagent Co., Ltd (China). Acetonitrile (ACN) was provided by Xilong Scientific Co., Ltd (China).

2.2. Synthesis of phthalimidoxy-1,3,5-triazine (TPT)

A novel nitrogen-oxygen compound, phthalimidoxy-1,3,5-triazine (TPT), was successfully synthesized by a one-pot method (Fig. 1a). In detail, N-hydroxyphthalimide (99.88 g, 0.6 mol), cyanuric chloride (37.25 g, 0.2 mol), and acetonitrile (200 mL) were added into a flask. A solution of triethylamine (20.44 g, 0.2 mol) in acetonitrile (50 mL) was added dropwise into the flask, and the reaction temperature was set to 25 °C (30 min), 45 °C (45 min), and 60 °C (60 min), respectively. After that, the mixture was heated to reflux for 2 h. Finally, the solid product was directly filtrated and washed with hot acetonitrile, followed by ultrasonic washing with deionized water to remove triethylamine hydrochloride. By drying at 105 °C for 4 h, the white TPT powder was obtained, with a yield of 85 %.

2.3. Preparation of flame retardant PA6 composites

Prior to processing, PA6 and TPT were dried separately in a vacuum oven at 80 °C for 8 and 4 h, respectively. TPT was then mechanically blended with PA6 at loading levels of 0.5, 1.0, and 1.5 wt %. The obtained samples were named in ascending order of the addition amount as PA6/0.5TPT, PA6/1TPT and PA6/1.5TPT, respectively. The mixtures were melt-compounded using a co-rotating twin-screw extruder, with the barrel temperature profile set to 220, 230, 235, 240, and 235 °C from the feeding zone to the die. The extrudates were water-cooled and pelletized, and the obtained flame-retardant PA6 pellets were further dried at 80 °C for 6 h under vacuum before injection molding into standard test specimens. Injection molding was performed using a temperature profile of 210, 220, 235, and 230 °C across the respective zones.

2.4. Characterizations

Fourier transform infrared (FTIR) spectroscopy was performed on a Spectrum 3 spectrometer to characterize TPT over the range of 500–4000 cm^{-1}. Nuclear magnetic resonance (NMR) spectroscopy was conducted on a Bruker AVANCE III HD 400 spectrometer to obtain ^{1}H and ^{13}C chemical shift data of TPT. Elemental analysis (EA) was performed on a UNICUBE analyzer to determine the C, H, O, and N contents of the samples, with results reported as mass percentages. X-ray photoelectron spectroscopy (XPS) analysis was carried out on a K-Alpha spectrometer to analyze the chemical states and elemental compositions of TPT.

TG-IR analysis was performed on a TGA 8000-Spectrum 3 system to investigate the thermal degradation behavior of TPT, PA6, and PA6/TPT composites. The samples were heated from 50 to 800 °C at a heating rate of 20 °C/min under nitrogen atmosphere with a flow rate of 40 mL/min. Pyrolysis-gas chromatography/mass spectrometry (Py-GC/MS) analysis was performed to identify the pyrolysis products of TPT, PA6 and PA6/TPT composites. The pyrolysis temperatures were set at 400 °C for TPT and 500 °C for both PA6 and PA6/TPT composites.

The UL-94 test was conducted on a CZF-5 horizontal and vertical burning tester according to the GB/T 2408–2021 standard, using specimens with dimensions of 130.0 mm × 13.0 mm and thicknesses of 3.2 mm, 1.6 mm, and 0.8 mm. The limiting oxygen index (LOI) was measured on a JF-3 oxygen index instrument according to the GB/T 2406.2–2009 standard, using specimens of 80.0 mm × 6.5 mm × 3.2 mm. Cone calorimetry test (CCT) was performed on a Fire Testing Technology 6810 cone calorimeter according to the ISO 5660–1:2015 standard, at a heat flux of 35 kW/m^2, using specimens of 90.0 mm × 90.0 mm × 4.0 mm.

X-ray diffraction (XRD) patterns of PA6 and PA6/TPT composites were recorded on a D8 ADVANCE diffractometer, with 2θ angles ranging from 5° to 90° at a scanning rate of 10 °/min. Differential scanning calorimetry (DSC) measurements were performed on a DSC 8000 instrument under nitrogen atmosphere to study the melting and crystallization behaviors of PA6 and PA6/TPT composites. Samples were heated from 45 to 250 °C at 10 °C/min, held at 250 °C for 3 min to erase thermal history, cooled to 45 °C at 10 °C/min to record the first cooling curve, and then reheated to 250 °C at the same rate to obtain the second heating curve. Dynamic mechanical analysis (DMA) was conducted on a DMA 8000 analyzer to assess the structural and molecular mobility of PA6 and PA6/TPT composites. The specimens (40.0 mm × 4.0 mm × 10.0 mm) were tested with a static force of 2 N, frequency of 1 Hz, amplitude of 0.05 mm, and temperature range of −50 to 150 °C at a heating rate of 2 °C/min. Mechanical properties were evaluated using an RGM 2030 universal testing machine. Tensile tests were conducted according to the GB/T 1040.1–2018 standard with specimen dimensions of 80.0 mm × 10.0 mm × 4.0 mm at a crosshead speed of 10 mm/min. Flexural tests were conducted in accordance with the GB/T 9341–2008 standard using the same specimen dimensions at a loading rate of 2 mm/min. The notched impact strength was determined according to the GB/T 1843–2008 standard using specimens of 80.0 mm × 10.0 mm × 4.0 mm. The notch was V-shaped and the depth was 2 mm.

The hygrothermal aging experiments of PA6 and PA6/1TPT were conducted in a KR - 880 type hygrothermal aging chamber. The samples were aged for 168 h at 85 °C and RH 85 %. After aging, the moisture in the samples was dried, and the samples were placed at 25 °C and RH 50 % for 24 h. Subsequently, the mechanical and flame-retardant properties of the samples were tested.

3. Results and discussion

3.1. Structural characterization of TPT

The structural characterization results of TPT are presented in Fig. 1 and S1 and Table S1. The ^{13}C NMR spectrum of TPT (Fig. 1b) exhibited five distinct carbon environments. The signals at 136.17, 127.89, and 124.55 ppm were assigned to the aromatic carbon atoms, while that at 161.12 ppm belonged to the carbonyl carbon. The chemical shift at 175.14 ppm was attributed to the carbon atoms of the triazine ring. Compared with the ^{13}C NMR of NHPI, the ^{13}C NMR spectrum of TPT revealed pronounced shifts for both the aromatic carbons and the carbonyl carbon, indicating successful substitution of chlorine atoms in cyanuric chloride by the phthalimidoxy groups. These obvious shifts were attributed to the strong electron-withdrawing effect and π-π conjugation of the triazine ring. The ^{1}H NMR spectrum of TPT (Fig. 1c) showed a multiplet at 7.81–7.89 ppm, corresponding to the aromatic protons. Compared with NHPI, the hydroxyl proton signal at 10.81 ppm completely disappeared, while the aromatic proton signals exhibited a slight downfield shift. These NMR results collectively demonstrate the successful synthesis of TPT.

Fig. 1d presents the FTIR spectra of TCT, TPT and NHPI. In the FTIR spectrum of TPT, the C—Cl stretching vibration peak completely disappeared at 848 cm^{-1} [29], confirming the substitution of chlorine atoms. Additionally, no O—H stretching vibrations were observed at 3537 and 3147 cm^{-1}, indicating the absence of hydroxyl groups. A new strong absorption peak appeared at 1057 cm^{-1}, belonging to the C—O stretching vibration. The formation of the C—O bond also led to a red shift of the *C=N* stretching vibration from 1486 to 1592 cm^{-1}, accompanied by a shift of the C–N stretching vibration from 1270 to 1300 cm^{-1} [29].

The XPS N1s, O1s and C1s spectra of TPT are shown in Fig. 1e-g. The N1s spectrum (Fig. 1e) exhibited two distinct peaks corresponding to *C=N* bond (399.5 eV) and C—N bond (401.4 eV), respectively. Similarly, the O1s spectrum (Fig. 1f) showed two distinct peaks at 534.8 and 531.5 eV, which were assigned to C—O and *C=O* bonds. Compared with the hydroxyl oxygen binding energy of NHPI (533.9 eV, Fig. S1), the upshift

to 534.8 eV indicates that the electron-deficient triazine ring decreases the electron density of the bonded oxygen atom, thereby increasing its O1s binding energy. The C1s spectrum (Fig. 1*g*) displayed a peak at 284.8 eV, which was assigned to *C*=*C* bond. Meanwhile, the peaks at 289.0 and 288.4 eV were attributed to *C*=*N* and *C*=*O* bonds, respectively [30].

The EA results of TPT are summarized in Table S1. The experimentally measured contents of C, H, O, and N were in close agreement with their theoretical values. All these results demonstrate the successful synthesis of TPT.

3.2. Thermal stability and thermal decomposition pathway of TPT

The TG and derivative TG curves of TPT (Fig. 2a) demonstrated an initial decomposition temperature (temperature at 1 % weight loss, $T_{1\ \%}$) of 322 °C, substantially exceeding the processing temperature of PA6, indicating its exceptional thermal stability [25]. Furthermore, TPT showed a char residue of 17.6 % at 800 °C, indicative of superior char-forming ability.

The Py-GC/MS results of TPT are shown in Fig. 2b, c and Table S2. Under heating, TPT produced substantial amounts of phthalimide and its derivatives, indicating preferential cleavage of its N—O bonds. This observation was corroborated by DFT calculations, which showed that the bond dissociation energy (BDE) of the N—O bond (72.0 kcal/mol) was lower than that of the C—O bond (90.5 kcal/mol), demonstrating the higher susceptibility of the N—O bond to thermal cleavage. Although TPT did not undergo the initially hypothesized C—O bond scission to generate nitroxyl radicals, it still exhibited excellent flame-retardant performance in PA6. Thus, we further investigated the flame-retardant mechanism of TPT, focusing on the radicals generated during its thermal decomposition, as detailed in *Section 3.6*.

3.3. Flame retardancy of PA6 and PA6/TPT composites

The flame retardant properties of PA6 and PA6/TPT composites are often characterized by the limiting oxygen index (LOI) and UL-94 tests [31]. The flame retardancy data of PA6 and PA6/TPT composites are shown in Fig. 3, S2 and Table S3. The total burning time of PA6/TPT composite gradually decreased with increasing TPT content (Fig. 3a). At the same TPT loading level, thinner specimens exhibited shorter total burning times. This is because thinner samples facilitate faster heat transfer, which accelerates the thermal decomposition of TPT and promotes the generation of radicals that effectively suppress the combustion chain reaction. The LOI of pure PA6 was only 22.9 % (Fig. 3b), while that of PA6/1.5TPT with 1.5 wt % of TPT increased to 28.0 %, indicating superior flame-retardant function of TPT. Meanwhile, the specimens after hygrothermal aging still maintained good flame retardancy (Table S4 and S5), indicating that TPT has certain application potential.

Cone calorimetry test (CCT) is widely applied to comprehensively investigate the combustion behaviors of materials under forced fire conditions [32]. CCT results demonstrated that the incorporation of TPT significantly extended the time to ignition (TTI) of PA6 composites (Fig. 3c). This is attributed to the radicals generated during TPT decomposition, which effectively scavenge active radicals (e.g., H·) during the early irradiation stage, thereby suppressing the initial thermal degradation of PA6 and delaying the release of flammable volatiles. This observation is consistent with TG results (Fig. 3d and e). Furthermore, the $T_{1\ \%}$ of PA6 (382 °C) was well-matched with the maximum decomposition temperature (T_{max} = 344 °C) of TPT, allowing the radicals generated from TPT to effectively suppress the initial decomposition of PA6. The mass loss rate, heat release rate and total heat release curves of PA6 and its composites are shown in Fig. S2. Although TPT cannot suppress the heat release of the PA6 matrix, it notably reduced the total smoke production (TSP, Fig. 3f). Thus, TPT primarily functions in the gas phase during the initial decomposition of PA6. However, after ignition, its decomposition products cannot exert condensed-phase effect to suppress the heat release, leading to the increased PHRR and THR (Table S6). Although TPT itself has relatively good char-forming ability, it cannot effectively catalyze the char formation of PA6 because it does

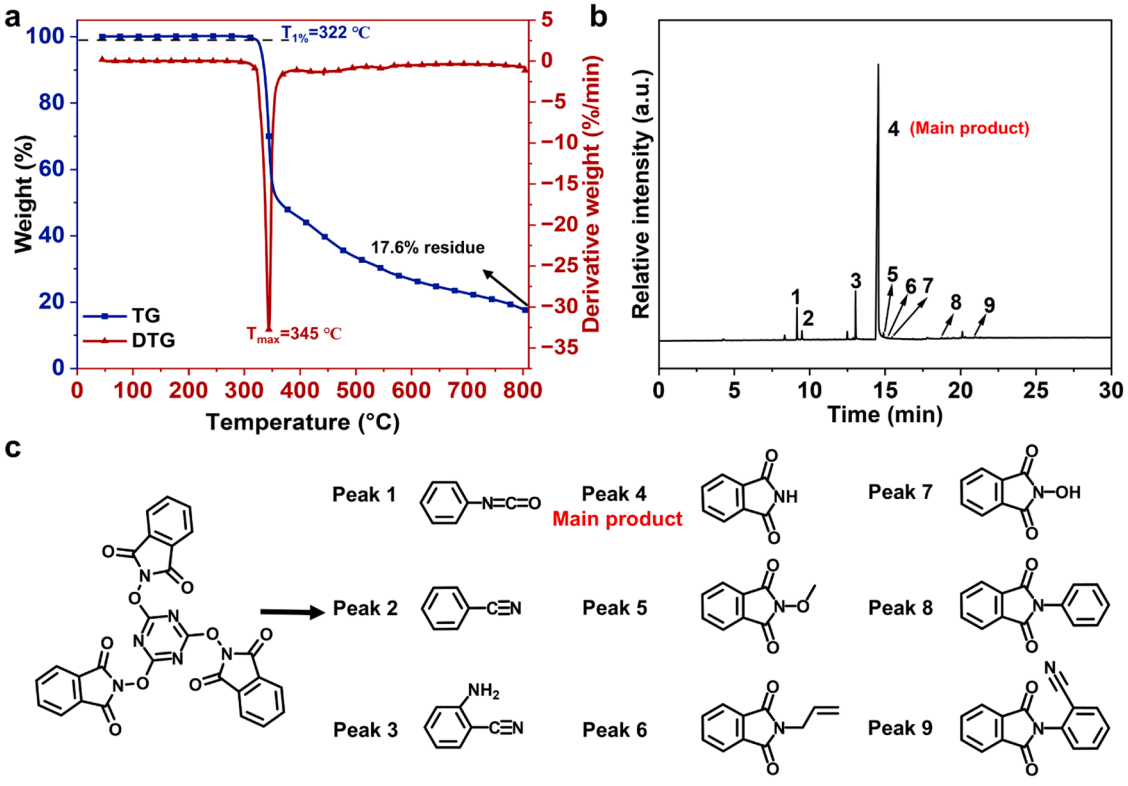

Fig. 2. (a) TG and DTG curves of TPT; (b) Py-GC/MS spectrum of TPT; and (c) Pyrolysis products of TPT.

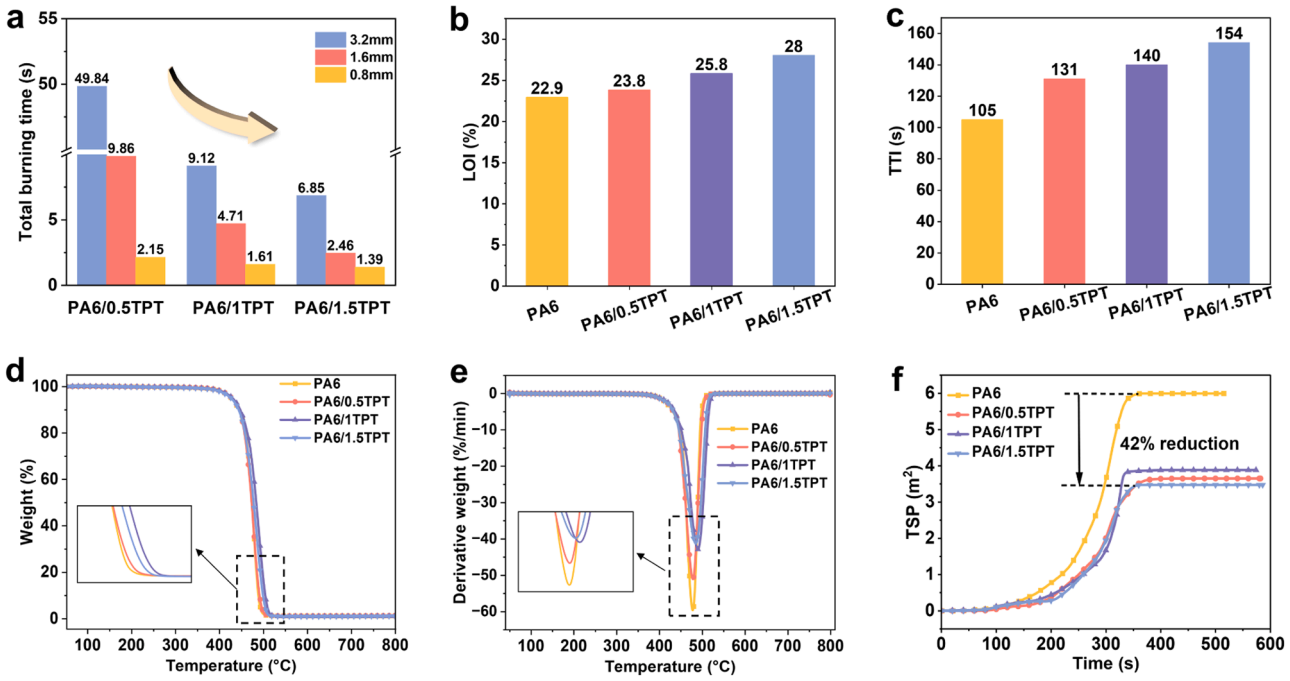

Fig. 3. (a) Total burning times during UL-94 test; (b) LOI values; (c) TTI values; (d) TG curves (e) DTG curves; and (f) TSP curves of PA6/TPT composites.

not contain an acid source. Therefore, in PA6, gaseous products are mainly generated rather than condensation char formation. Meanwhile, since the addition amount of TPT is extremely low, the char formed by itself cannot play a flame-retardant role. Moreover, after the gaseous products capture free radicals, they may participate in the combustion process. As a result, it is unable to reduce the THR and PHRR. Nevertheless, in real fire scenarios, inhalation of toxic smoke is a major threat to human life. Therefore, the extended TTI and reduced TSP are critical for increasing the probability of successful fire escape. According to the literature [33], the fire performance index (FPI) is the ratio of TTI to PHRR. The higher the FPI, the lower the fire hazard. Therefore, by calculating the FPI values of different PA6/TPT composite materials and finding the balance point between TTI and PHRR, it is more conducive to reducing the fire hazard.

3.4. Mechanical properties of PA6 and PA6/TPT composites

Conventional flame retardants typically lead to deterioration in the mechanical properties of PA6. In contrast, the PA6/TPT composites demonstrated significantly enhanced tensile strength and flexural strength and well-preserved impact strength (Fig. 4a-c). The introduction of 1.5 wt % of TPT resulted in enhancements of 17.3 % and 18.1 % in tensile strength and flexural strength, respectively. As shown in Fig. 4d-f, the storage modulus, loss modulus, and damping factor (tanδ) of PA6/TPT composites were all increased compared to pure PA6, indicating improved rigidity and damping capacity. This behavior can be attributed to TPT acting as an effective heterogeneous nucleating agent, significantly increasing the number of microcrystals within PA6. These microcrystals function as physical cross-linking points within PA6, substantially enhancing the rigidity and energy storage capability. The increased number of crystal-amorphous interfaces provides additional frictional resistance to chain segment movement, thereby strengthening the energy dissipation capacity in the glass transition region. As TPT does not form chemical cross-links with PA6, it cannot restrict the mobility of the PA6 chain segments, thus the glass transition temperature (T_g) of PA6 composites was unchanged.

To study the influence of TPT in actual use on the mechanical properties of PA6, we conducted hygrothermal aging experiments on PA6 and PA6/1TPT. The results showed that the mechanical properties of the samples after the hygrothermal aging experiments all decreased, but the addition of TPT did not lead to an increase in the degree of decline (Table S7). This indicated that TPT remained stable during the aging process of PA6 and did not damage the mechanical properties of PA6. It also proves that TPT has certain application potential in PA6.

As a typical semi-crystalline polymer, the crystallization behavior of PA6 significantly influences its mechanical properties. Therefore, DSC and XRD were employed to systematically investigate the melting and crystallization behaviors of PA6/TPT composites. The second heating curve of PA6 exhibited two melting peaks (Fig. 4*g*), which can be attributed to a melt-recrystallization mechanism [34]. The increased melting enthalpy of PA6/TPT composites indicated that TPT enhanced the crystallinity of PA6, while its elevated crystallization temperature (T_c) further confirmed the role of TPT as a nucleating agent in promoting the crystallization of PA6. As shown in Fig. 4i, pure PA6 mainly exhibited the γ-crystal form, with its (001) plane corresponding to $2\theta = 21.3°$, resulting from non-equilibrium crystallization during rapid cooling. After the incorporation of TPT, a new diffraction peak appeared at $2\theta = 22.9°$, which was assigned to the (002) plane of the α-crystal form of PA6 [35]. The intensity of this diffraction peak increased with increasing TPT content, demonstrating that TPT facilitated the transition of PA6 to the more stable α-crystal form. In contrast, the α-crystal form has a more compact and regular molecular chain arrangement, a more continuous hydrogen bond network, and higher rigidity. Meanwhile, the γ-crystal form has greater toughness and ductility. Therefore, an increase in the proportion of the α-crystal type will lead to a slight decrease in the impact strength of the PA6/TPT composites.

3.5. Gas-phase decomposition products of PA/1.5TPT

TG-FTIR and Py-GC/MS were employed to characterize the gas-phase decomposition behavior of PA6 and PA6/1.5TPT. As shown in Fig. 5a-c, the gaseous products of both samples were essentially identical, primarily consisting of hydrocarbons (2938 cm^{-1}), carbonyl compounds (1712 cm^{-1}), H_2O (3444 cm^{-1}), and CO_2 (2354 cm^{-1}) [36,37]. Thus, the addition of TPT did not alter the decomposition pathway of PA6. However, the release intensity of these gaseous products for

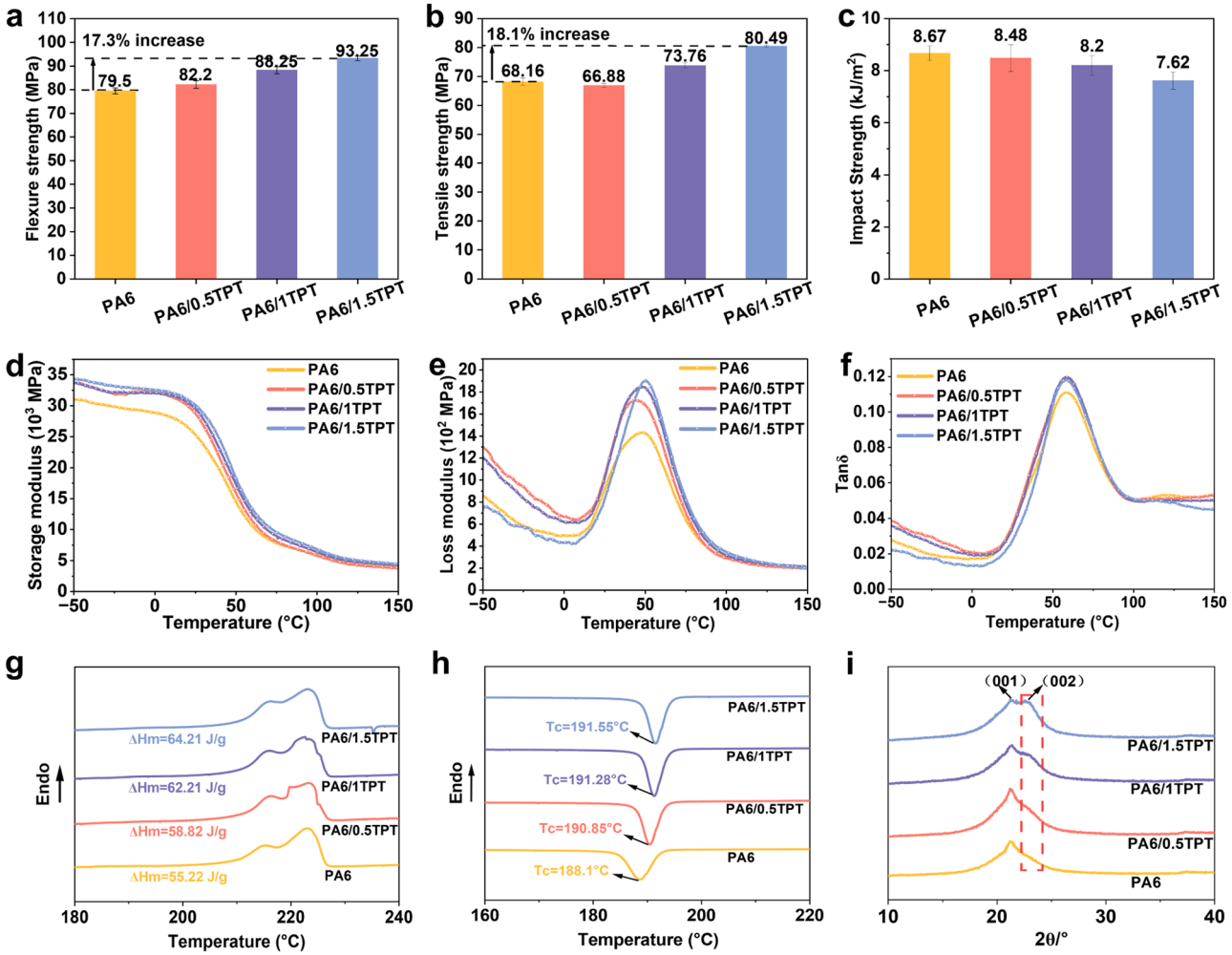

Fig. 4. (a) Tensile strength; (b) Flexure strength; (c) Impact strength; (d) Storage modulus curves; (e) Loss modulus curves; (f) Tan δ curves; (g) 2nd heating curves; (h) 1st cooling curves; and (i) XRD patterns of PA6 and PA6/TPT composites.

PA6/1.5TPT was significantly reduced. The suppression effect of TPT towards the decomposition of PA6 could also be confirmed in Fig. 5d and e. Fig. 5f and Table S9 further confirm the high similarity in pyrolysis products between PA6 and PA6/TPT composites. A simplified pyrolysis pathway is proposed in Fig. 5g Under heating, PA6 mainly undergoes α-scission followed by intramolecular cyclization and dehydration to form carbonyl compounds and long-chain nitriles, consistent with literature reports [38]. The yield of the main product, ε-caprolactam, decreased with increasing TPT content. The integrated analysis of TG-FTIR and Py-GC/MS results demonstrates that TPT exerts a significant inhibitory effect on the degradation of molecular chains during the pyrolysis of PA6.

3.6. Flame retardant mechanism of TPT

The above results reveal that TPT exerts a gas-phase flame retardant effect by generating radicals to capture high-energy radicals released in the initial degradation of PA6, thereby suppressing polymer chain degradation. As the decomposition products of TPT are radicals themselves, they must exhibit moderate stability to participate efficiently in radical capture. If their stability is too low, these radicals may rapidly deactivate, failing to scavenge active species and potentially triggering side reactions within the polymer matrix. Conversely, if the radicals are excessively stable, their reactivity would be insufficient, resulting in reduced scavenging efficiency and diminished flame retardant performance. To assess the stability of TPT-derived radicals, we calculated their HOMO-LUMO orbital energies and energy gaps (ΔE). As shown in Fig. 6a, the ΔE values for TPT, phthalimide N-radicals, and triazine oxy-radicals are 4.91, 4.84, and 5.03 eV, respectively. The relatively high ΔE value of TPT indicates its inherent stability [39], while the similar ΔE values of its decomposition products confirm that the resulting radicals possess appropriate stability and are sufficient to persist under thermal conditions to fulfill the requirements for effective radical scavenging.

According to literature reports [26,40,41], the weakest bond in PA6 chains during thermo-oxidative degradation is the C—H bond at the N-adjacent methylene group. Cleavage of this C—H bond during initial degradation generates H· and carbon radicals, initiating a series of reactions that lead to rapid degradation of PA6. Thus, the flame retardant mechanism of TPT involves the phthalimide N-radicals and triazine oxy-radicals generated during pyrolysis capturing the H· and C· radicals to suppress the early degradation of PA6 (Fig. 6b). To evaluate the thermodynamic feasibility of these pathways, the Gibbs free energy changes (ΔG) and enthalpy changes (ΔH) for these reactions were calculated. Additionally, the tendency for hydrogen abstraction from PA6 molecular chains by the decomposition products of TPT was computationally investigated. All calculations were performed using first-principles methods based on DFT, implemented through the Vienna Ab initio Simulation Package (VASP) in conjunction with Gaussian software. Geometry optimisations were performed using Gaussian 16, employing the B3LYP functional [42] and 6–31G(d) [43] basis set. The geometry optimisations were run with dispersion corrections from Grimme's D3 model [44] with Becke-Johnson damping factors [45].

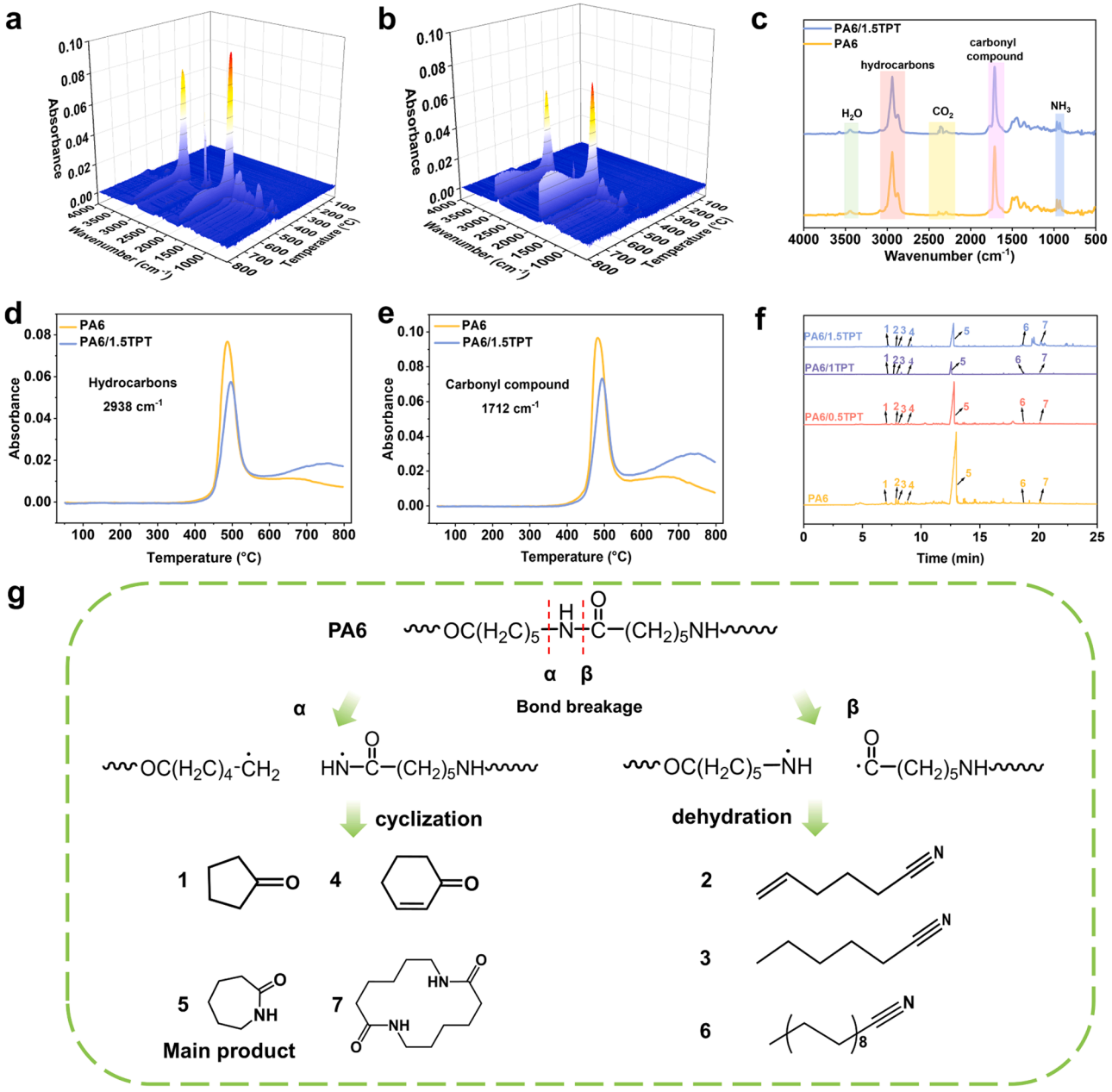

Fig. 5. 3D TG-FTIR spectra of (a) PA6 and (b) PA6/1.5TPT; (c) FTIR spectra of degradation products of PA6 and PA6/1.5TPT at T_{max}; (d) Real-time absorption peak curves of (d) hydrocarbons (e) carbonyl compounds; (f) Py-GC/MS spectra of PA6 and PA6/TPT composites; and (g) pyrolysis process of PA6.

Harmonic vibrational frequencies calculations were performed to confirm the stationary points as true minima or transition states, as well as to provide thermodynamic corrections to the SCF energies. The calculation of single-point energy used wB7 xd functional and def2-TZVP basis set. The Gibbs free energy of each molecule was obtained using frequency correction shown by Gaussview.

The DFT calculation results (Fig. 6c) revealed that the ΔG for hydrogen abstraction from the N-adjacent methylene group of PA6 by phthalimide N-radicals and triazine oxy-radicals were −31.54 and −28.95 kcal/mol, respectively. This indicates that thermodynamically, the decomposition products of TPT still possess a tendency to abstract hydrogen atoms from the N-adjacent methylene groups in PA6 chains, which might potentially promote PA6 degradation. This finding partially explains the increases in PHRR and THR along with the decrease in TSP. However, the ΔG values for the reactions of phthalimide N-radicals with free H· and C· radicals were −112.06 and −101.28 kcal/mol, while those for triazine oxy-radicals with H· and C· were −109.46 and −117.36 kcal/mol. These values are much more negative than the ΔG values for hydrogen abstraction reactions, demonstrating that both radicals preferentially capture active radicals (H· and C·) in the system to form more stable products. The driving force for these radical scavenging reactions is substantially stronger than that for hydrogen abstraction from PA6. These conclusions are further supported by the calculated ΔH shown in Fig. S3. Therefore, during PA6 decomposition, TPT primarily exerts a gas-phase effect through the efficient capture of active radicals by its phthalimide N-radicals and triazine oxy-radicals, thereby inhibiting the scission and degradation of polymer molecular chains.

4. Conclusions

In this work, a triazine-based nitrogen-oxygen compound (TPT) was

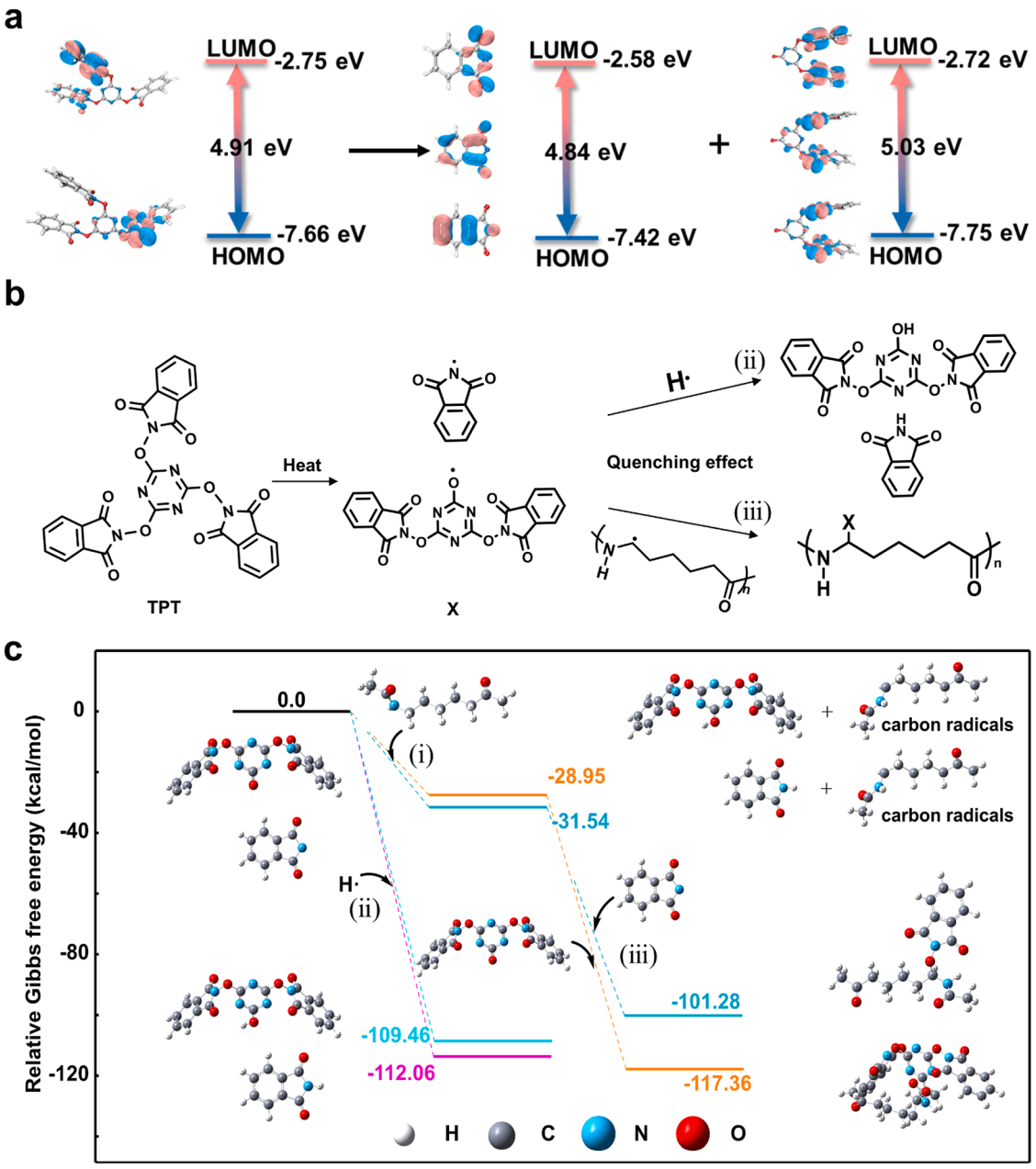

Fig. 6. (a) The HOMO and LUMO orbital energies, along with the corresponding energy gap differences, for TPT and its decomposition products; (b) Flame retardant mechanism of TPT; and (c) The Gibbs free energy change for the reactions between TPT decomposition products and (i) N-adjacent αH, (ii) H·, and (iii) C.

synthesized through the reaction between TCT and NHPI. Our results confirmed that the thermal decomposition of TPT primarily involved homolytic cleavage of the N—O bond, generating phthalimide N- and triazine oxy-radicals. Even at low loading levels, TPT significantly reduced the combustion time of PA6 and increased the LOI. Meanwhile, introducing TPT can extend TTI of PA6 and decrease TSP, thereby prolonging the critical escape time in fire scenarios. During combustion, the stable phthalimide N-radicals and triazine oxy-radicals derived from TPT effectively captured active radicals (e.g., H· and C·) generated during the initial degradation of PA6, forming more stable products and consequently interrupting the radical chain reactions in gas phase. The hygrothermal aging test indicated that under high-temperature and high-humidity conditions, TPT still maintained a good flame-retardant effect and did not damage the mechanical properties of PA6. This work introduces an efficient flame-retardant strategy that also enhances mechanical properties, highlighting the potential of nitrogen-oxygen compounds for flame-retardant PA6.

CRediT authorship contribution statement

Ruiqi Liu: Writing – original draft, Visualization, Methodology, Formal analysis. **Bin Tao:** Writing – review & editing, Validation, Investigation. **Suliang Gao:** Data curation. **Miaojun Xu:** Supervision, Resources, Project administration, Funding acquisition. **Siqi Huo:** Writing – review & editing, Funding acquisition, Formal analysis. **Xiaoli Li:** Funding acquisition, Conceptualization. **Bin Li:** Supervision, Resources.

Declaration of competing interest

The authors declare that they have no known competing financial interests or personal relationships that could have appeared to influence

the work reported in this paper.

Acknowledgments

This work was financially supported by the National Natural Science Foundation of China (52173069 and 52473071), the Fundamental Research Funds for the Central Universities (2572025JT10), the Key Research and Development Projects in Heilongjiang Province (2024ZXDXA29) and the Australian Research Council (DE230100616).

Supplementary materials

Supplementary material associated with this article can be found, in the online version, at doi:10.1016/j.polymdegradstab.2026.111924.

Data availability

Data will be made available on request.

References

[1] B. Wang, X. Li, Z. Hu, S. Wang, W. Dong, B. Wang, L. Wang, N. Gong, Functionalization of aluminum alloy surface with reactive epoxide silane to induce ultra-high strength polyamide 6 /aluminum alloy composite joint, Appl. Surf. Sci. 626 (2023) 157231, https://doi.org/10.1016/j.apsusc.2023.157231.
[2] M. Qian, X. Xu, Z. Qin, S. Yan, Silicon carbide whiskers enhance mechanical and anti-wear properties of PA6 towards potential applications in aerospace and automobile fields, Compos. Pt. B-Eng 175 (2019) 107096, https://doi.org/10.1016/j.compositesb.2019.107096.
[3] S. Marais, Q. Lozay, N. Follain, J. Soulestin, N. Couvrat, E. Dargent, Multinanolayered PA6/cloisite and PE/PA6/cloisite composites: structure, mechanical and barrier properties, Compos. Pt. B-Eng. 271 (2024) 111167, https://doi.org/10.1016/j.compositesb.2023.111167.
[4] K. Olonisakin, A. Rodriguez-Uribe, T. Wang, A.K. Mohanty, M. Thimmanagari, M. Misra, Engineered advanced light-weight sustainable composites from surface modified recycled carbon fiber reinforced polyamide 6,6 for metallic part alternative in automotive, Compos. Pt. B-Eng. 300 (2025) 112375, https://doi.org/10.1016/j.compositesb.2025.112375.
[5] B. Tawiah, S. Ullah, Z. Cheng, M.Z. Rahman, Y. Ming, D. Chen, C.K. Kundu, W. Cai, A.C. Yuen, B. Yu, Z. Guangping, B. Amirbek, B. Fei, Microporous transition metal phosphide flame retardant toughened PA6 composites with excellent thermal conductivity and ferroelectric response, Compos. Pt. B-Eng. 300 (2025) 112502, https://doi.org/10.1016/j.compositesb.2025.112502.
[6] Y. Wang, L. Cui, J. Zhang, J. Shen, H. Xu, Z. Zhou, Y. Li, M. Zhu, Fire retardant treatments for polyamide 6 and 66: advances and trends over the last five years, ACS Appl. Polym. Mater. 7 (2025) 4677–4693, https://doi.org/10.1021/acsapm.5c00291.
[7] S. Fan, B. Peng, R. Yuan, D. Wu, X. Wang, J. Yu, F. Li, A novel Schiff base-containing branched polysiloxane as a self-crosslinking flame retardant for PA6 with low heat release and excellent anti-dripping performance, Compos. Pt. B-Eng. 183 (2020) 107684, https://doi.org/10.1016/j.compositesb.2019.107684.
[8] J. Feiteiro, M. Mariana, E. Cairrão, Health toxicity effects of brominated flame retardants: from environmental to human exposure, Environ. Pollut. 285 (2021) 117475, https://doi.org/10.1016/j.envpol.2021.117475.
[9] L. Khani, L. Martin, Ł. Pułaski, Cellular and physiological mechanisms of halogenated and organophosphorus flame retardant toxicity, Sci. Total Environ. 897 (2023) 165272, https://doi.org/10.1016/j.scitotenv.2023.165272.
[10] Y. Xu, S. Liang, W. Wang, C. Yan, L. Liu, D. Jiang, M. Hong, M. Xu, B. Li, S. Huo, Truss-inspired ultra-high strength, fire-safe, and thermal insulating double-crosslinked wood aerogels, J Mater Sci Technol 259 (2026) 268–278, https://doi.org/10.1016/j.jmst.2025.09.044.
[11] C. Wang, S. Huo, G. Ye, C.-F. Cao, M. Hong, Y.-T. Pan, P. Song, H. Wang, T. Wang, Z. Liu, Tick-inspired, self-healing, and strongly-adhesive coatings with biodegradability and phosphorus-free fire retardancy, J Mater Sci Technol 260 (2026) 229–240, https://doi.org/10.1016/j.jmst.2025.10.003.
[12] T. Sai, X. Ye, B. Wang, Z. Guo, J. Li, Z. Fang, S. Huo, Transparent, intrinsically fire-safe yet impact-resistant poly(carbonates-b-siloxanes) containing schiff-base and naphthalene-sulfonate, J Mater Sci Technol 225 (2025) 11–20, https://doi.org/10.1016/j.jmst.2024.11.023.
[13] G. Fei, Y. Liu, Q. Wang, Synergistic effects of novolac-based char former with magnesium hydroxide in flame retardant polyamide-6, Polym. Degrad. Stab. 93 (2008) 1351–1356, https://doi.org/10.1016/j.polymdegradstab.2008.03.031.
[14] B. Wang, R. Ye, Z. Guo, J. Li, Z. Fang, S. Ran, Thermal stability and fire safety of polycarbonate flame retarded by the brominated flame retardant and a non-antimony synergistic agent, J. Polym. Res. 30 (2023) 240, https://doi.org/10.1007/s10965-023-03586-w.
[15] E.A. Haidasz, D. Meng, R. Amorati, A. Baschieri, K.U. Ingold, L. Valgimigli, D. A. Pratt, Acid is key to the radical-trapping antioxidant activity of nitroxides, J. Am. Chem. Soc. 138 (2016) 5290–5298, https://doi.org/10.1021/jacs.6b00677.
[16] G. Gryn'ova, K.U. Ingold, M.L. Coote, New insights into the mechanism of amine/nitroxide cycling during the hindered amine light stabilizer inhibited oxidative degradation of polymers, J. Am. Chem. Soc. 134 (2012) 12979–12988, https://doi.org/10.1021/ja3006379.
[17] I. Vulic, J. Eng, S.B. Samules, A.H. Wagner, New breakthroughs in hindered amine light stabilizer performance, Polym. Polym. Compos. 7 (1999) 565–573, https://doi.org/10.1177/096739119990708565.
[18] W. Ma, M. Meng, X. Jiang, B.-T. Tang, S.-F. Zhang, Synthesis of a water-soluble macromolecular light stabilizer containing hindered amine structures, Chin. Chem. Lett. 24 (2013) 153–155, https://doi.org/10.1016/j.cclet.2013.01.026.
[19] T. Jiang, J. Zhang, Comparison of UV resistance of HDPE added with hindered amine light stabilizers with different molecular structures, Polym. Adv. Technol. 32 (2020) 1288–1300, https://doi.org/10.1002/pat.5177.
[20] P.D. Evans, S. Kraushaar Gibson, I. Cullis, C. Liu, G. Sèbe, Photostabilization of wood using low molecular weight phenol formaldehyde resin and hindered amine light stabilizer, Polym. Degrad. Stab. 98 (2013) 158–168, https://doi.org/10.1016/j.polymdegradstab.2012.10.015.
[21] X. Di, X. Chen, Y. Kang, J. Yang, Y. Zou, J. Jing, J. Sun, H. Li, X. Gu, S. Zhang, Introducing a polysiloxane coating on flame retardant to realize durable UV resistance and flame retardancy of polypropylene, Polym. Degrad. Stab. 239 (2025) 111403, https://doi.org/10.1016/j.polymdegradstab.2025.111403.
[22] R. Ma, M. Zhao, Y. Mo, P. Tang, Y. Feng, D. Li, HALS intercalated layered double hydroxides as an efficient light stabilizer for polypropylene, Appl. Clay Sci. 180 (2019) 105196, https://doi.org/10.1016/j.clay.2019.105196.
[23] X. Wang, M. Xu, Z. Zhang, Y. Leng, B. Li, Synthesis of a novel N-alkoxyamine containing compound and its application as an effective flame retardant for polypropylene film by quenching free radical, J. Anal. Appl. Pyrolysis 134 (2018) 243–253, https://doi.org/10.1016/j.jaap.2018.06.014.
[24] H. Xie, X. Lai, R. Zhou, H. Li, Y. Zhang, X. Zeng, J. Guo, Effect and mechanism of N-alkoxy hindered amine on the flame retardancy, UV aging resistance and thermal degradation of intumescent flame retardant polypropylene, Polym. Degrad. Stab. 118 (2015) 167–177, https://doi.org/10.1016/j.polymdegradstab.2015.04.022.
[25] C. El-Mazry, M. Ben Hassine, O. Correc, X. Colin, Thermal oxidation kinetics of additive free polyamide 6-6, Polym. Degrad. Stab. 98 (2013) 22–36, https://doi.org/10.1016/j.polymdegradstab.2012.11.002.
[26] P. Ren, T. Li, L. Feng, X. Gu, M. Jiang, J. Duan, C. Zhang, Thermal degradation of polyamide 6: mechanisms, mitigation strategies, and challenges, Chem. Eng. Sci. 316 (2025) 121985, https://doi.org/10.1016/j.ces.2025.121985.
[27] R. Li, X. Hu, Study on discoloration mechanism of polyamide 6 during thermo-oxidative degradation, Polym. Degrad. Stab. 62 (1998) 523–528, https://doi.org/10.1016/S0141-3910(98)00037-8.
[28] B. Spieß, E. Metzsch-Zilligen, R. Pfaendner, A new class of oxyimides: oxyimide ethers and their use as flame retardants, Macromol. Mater. Eng. 306 (2021) 2000650, https://doi.org/10.1002/mame.202000650.
[29] Q. Chen, J. Zhang, J. Li, J. Sun, B. Xu, H. Li, X. Gu, S. Zhang, Synthesis of a novel triazine-based intumescent flame retardant and its effects on the fire performance of expanded polystyrene foams, Polym. Degrad. Stab. 203 (2022) 110079, https://doi.org/10.1016/j.polymdegradstab.2022.110079.
[30] S. Liu, Y. Qiu, T. Wang, D. Li, L. Qian, W. Xi, J. Wang, L. Qu, W. Tang, Intumescent flame retardant behavior of aryl Schiff base triazine piperazine char-forming agent with heat-induced cyclization self-crosslinking trait in polypropylene, Chem. Eng. J. 508 (2025) 160959, https://doi.org/10.1016/j.cej.2025.160959.
[31] Y. Guo, Q. Yang, S. Huo, J. Li, P. Jafari, Z. Fang, P. Song, H. Wang, Recyclable fire-retardant bio-based thermosets: from molecular engineering to performances and applications, Prog. Polym. Sci. 162 (2025) 101935, https://doi.org/10.1016/j.progpolymsci.2025.101935.
[32] Y. Guo, N. Song, S. Huo, C. Wang, G. Ye, M. Hong, Y.T. Pan, T. Chen, Z. Chen, Y. Yu, P. Song, H. Wang, Strong, recyclable, bio-based vitrimers by tailored rigid-flexible structures for advanced carbon fiber-reinforced polymers, Adv. Sci (2025) e13935, https://doi.org/10.1002/advs.202513935.
[33] H. Wang, A. Qin, C. Yan, K. Xu, Y. Xu, Y. Gang, B. Li, L. Liu, Molecular design of different phosphorus-containing groups on the mechanism of fire retardancy, compatibility and mechanics of thermoplastic polyurethanes, Chem. Eng. J. 522 (2025) 168019, https://doi.org/10.1016/j.cej.2025.168019.
[34] Y. Li, X. Zhu, G. Tian, D. Yan, E. Zhou, Multiple melting endotherms in melt-crystallized nylon 10,12, Polym. Int. 50 (2001) 677–682, https://doi.org/10.1002/pi.682.
[35] Z. Huang, Q. Yin, Q. Wang, P. Wang, T. Liu, L. Qian, Mechanical properties and crystallization behavior of three kinds of straws/nylon 6 composites, Int. J. Biol. Macromol. 103 (2017) 663–668, https://doi.org/10.1016/j.ijbiomac.2017.05.121.
[36] B. Liu, D. He, Z. Wang, H. Li, X. Fang, T. Ding, W. Zhang, Z. Li, Synergistic enhancement of flame retardancy and interfacial adhesion in glass fiber-reinforced polyamide 6 composites via DOPO-functionalized maleic anhydride copolymer, Chem. Eng. J. 522 (2025) 167686, https://doi.org/10.1016/j.cej.2025.167686.
[37] Y. Sun, X. Pei, Z. Wang, D. Wu, X. Wang, J. Yu, R. Yuan, F. Li, A macromolecular flame retardant for polyamide 6 and its filaments with enhanced fire safety, tensile and UV-blocking performance, Compos. Pt. B-Eng. 283 (2024) 111631, https://doi.org/10.1016/j.compositesb.2024.111631.
[38] Z. Wang, A. Liu, Y. Li, J. Yu, R. Yuan, F. Li, Synthesis and application of recyclable plant-based benzimidazole phytate for flame retardant PA6 filaments with excellent anti-dripping performance, Polym. Degrad. Stab. 241 (2025) 111550, https://doi.org/10.1016/j.polymdegradstab.2025.111550.
[39] C.V. Rajput, N.V. Sastry, N.P. Chikhaliya, Phosphorous-containing flame retardant plasticizer based on Cassia fistula seed oil and their application in poly(vinyl chloride) films, Ind. Crops Prod. 203 (2023) 117120, https://doi.org/10.1016/j.indcrop.2023.117120.

[40] T. Karstens, V. Rossbach, Thermo-oxidative degradation of polyamide 6 and 6,6. Kinetics of the formation and inhibition of UV/VIS-active chromophores, Macromol. Chem. Phys. 190 (2003) 3033–3053, https://doi.org/10.1002/macp.1989.021901201.
[41] Y. Shu, L. Ye, T. Yang, Study on the long-term thermal-oxidative aging behavior of polyamide 6, J. Appl. Polym. Sci. 110 (2008) 945–957, https://doi.org/10.1002/app.28647.
[42] A.D.J. Becke, Density-functional thermochemistry. III. The role of exact exchange, Chem. Phys. 98 (1993) 5648–5652, https://doi.org/10.1063/1.464913.
[43] C. Lee, W. Yang, R.G. Parr, Development of the Colle-Salvetti correlation-energy formula into a functional of the electron density, Phys. Rev. B: Condens. Matter Mater. Phys. 37 (1988) 785–789, https://doi.org/10.1103/physrevb.37.785.
[44] S. Grimme, J. Antony, S. Ehrlich, H. Krieg, A consistent and accurate ab initio parametrization of density functional dispersion correction (DFT-D) for the 94 elements H-Pu, J. Chem. Phys. 132 (2010) 154104, https://doi.org/10.1063/1.3382344.
[45] E.R. Johnson, A.D. Becke, A post-Hartree-Fock model of intermolecular interactions: inclusion of higher-order corrections, J. Chem. Phys. 124 (2006) 174104, https://doi.org/10.1063/1.2190220.